Mechanistic Study of the $CH_3O_2^\bullet + HO_2^\bullet \rightarrow CH_3O_2H + O_2$ Reaction in the Gas Phase. Computational Evidence for the Formation of a Hydrogen-Bonded Diradical Complex

Josep M. Anglada,[†] Santiago Olivella,*[,†] and Albert Solé[‡]

Institut d'Investigacions Químiques i Ambientals de Barcelona, CSIC, Jordi Girona 18, 08034-Barcelona, Catalonia, Spain, and Centre Especial de Recerca en Química Teòrica i Departament de Química Física, Universitat de Barcelona, Martí i Franquès 1, 08028-Barcelona, Catalonia, Spain

Received: February 7, 2006; In Final Form: March 16, 2006

In an attempt to understand the mechanism of the reaction of alkylperoxy radicals with hydroperoxy radical, a key reaction in both atmospheric and combustion chemistry, the singlet and triplet potential energy surfaces (PESs) for the gas-phase reaction between $CH_3O_2^\bullet$ and $HO_2^\bullet$ leading to the formation of CH_3OOH and O_2 have been investigated by means of quantum-mechanical electronic structure methods (CASSCF and CASPT2). In addition, standard transition state theory calculations have been carried out with the main purpose of a qualitative description of the strong negative temperature dependence observed for this reaction. All the pathways on both the singlet and triplet PESs consist of a reversible first step involving the barrierless formation of a hydrogen-bonded prereactive complex, followed by the irreversible formation of products. This complex is a diradical species where the two unpaired electrons are not used for bonding and is lying about 5 kcal/mol below the energy of the reactants at 0 K. The lowest energy reaction pathway occurs on the triplet PES and involves the direct H-atom transfer from HO_2 to CH_3O_2 in the diradical complex through a transition structure lying 3.8 kcal/mol below the energy of the reactants at 0 K. Contradicting the currently accepted interpretation of the reaction mechanism, the observed strong negative temperature dependence of the rate constant is due to the formation of the hydrogen-bonded diradical complex rather than a short-lived tetraoxide intermediate CH_3OOOOH.

1. Introduction

Alkylperoxy radicals play important roles as reaction intermediates in the tropospheric oxidation and combustion of hydrocarbons (RH).[1−5] These processes are initiated mainly by the attack of hydroxyl radical ($HO^\bullet$). As a hydrogen atom is abstracted, an alkyl radical ($R^\bullet$) forms (eq 1), and the subsequent addition of molecular oxygen (O_2, $^3\Sigma_g^-$), designated by $^3O_2$, to $R^\bullet$ yields an alkylperoxy radical ($RO_2^\bullet$) (eq 2). The alkylperoxy

$$RH + HO^\bullet \rightarrow R^\bullet + H_2O \quad (1)$$

$$R^\bullet + {}^3O_2 \rightarrow RO_2^\bullet \quad (2)$$

radicals generally exhibit low reactivity toward closed shell molecular species, and, consequently, they essentially react with themselves and with other radical species. When nitrogen oxides are present in low concentration, the reactions of alkylperoxy radicals with hydroperoxy radical ($HO_2^\bullet$) are among the most important combination reactions of alkylperoxy radicals.[6] This importance results from the abundance of $HO_2^\bullet$, which can be formed from various sources in the atmospheric oxidation of hydrocarbons.

The $RO_2^\bullet + HO_2^\bullet$ reactions are generally rapid, with rate constants at room temperature in the range $(5-20) \times 10^{-12}$ cm^3 molecule^{-1} s^{-1}, and, therefore, contribute significantly to the chemistry of alkyl peroxy radicals.[6,7] The only product of reaction of unsubstituted alkylperoxy radicals $RO_2^\bullet$ (e.g., $CH_3O_2^\bullet$, $C_2H_5O_2^\bullet$, etc.) with $HO_2^\bullet$ that has been characterized is the alkyl hydroperoxide ROOH (eq 3). This reaction is chain terminating because ROOH is stable under atmospheric conditions. For instance, the methylperoxy radical ($CH_3O_2^\bullet$) and $HO_2^\bullet$

$$RO_2^\bullet + HO_2^\bullet \rightarrow ROOH + O_2 \quad (3)$$

react giving methyl hydroperoxide (CH_3OOH) in 100% yield (eq 4), which can be removed from the troposphere via precipitation.[1,2,6] Understanding the kinetics and mechanism of

$$CH_3O_2^\bullet + HO_2^\bullet \rightarrow CH_3OOH + O_2 \quad (4)$$

$RO_2^\bullet + HO_2^\bullet$ reactions is therefore crucial to model the oxidation processes of hydrocarbons under atmospheric conditions.

The temperature dependence of $RO_2^\bullet + HO_2^\bullet$ reactions has been investigated by several groups, and these studies all report strong negative temperature dependences, namely, the rate at which $RO_2^\bullet$ is consumed decreases with increasing temperature.[1−4] This observation suggests that a major fraction of the reaction proceeds via channel(s) that involve the formation of a short-lived tetraoxide intermediate (ROOOOH), which can either dissociate into the reactants or react to form the products. The $RO_2^\bullet + HO_2^\bullet$ reactions are thought to proceed via the mechanistic pathways given in Scheme 1 ($CH_3O_2^\bullet$ used as example).[2] Pathway "A" involves the formation of a loosely bound tetraoxide adduct, CH_3OOOOH, which either decomposes back to reactants or rearranges yielding CH_3OOH and O_2 through a four-membered-ring transition state in which the methyl group

* Corresponding author. E-mail: sonqtc@cid.csic.es.
[†] Institut d'Investigacions Químiques i Ambientals de Barcelona.
[‡] Centre Especial de Recerca en Química Teòrica and Departament de Química Física.

10.1021/jp060798u CCC: $33.50
Published on Web 04/18/2006

SCHEME 1

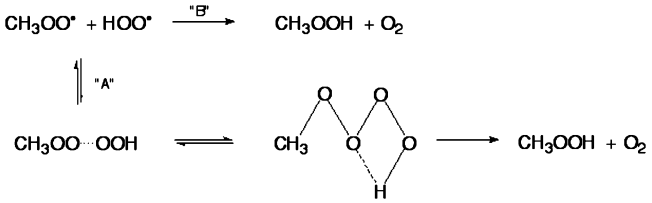

does not participate itself. However, the nature of the postulated tetraoxide intermediate is still uncertain and is open to speculation. Pathway "B" consists of a simple direct H-atom transfer from $HO_2^\bullet$ to $CH_3O_2^\bullet$ and is thought to be a channel of minor importance. Nevertheless, it is possible that both pathways contribute to the overall rate constant of the $CH_3O_2^\bullet + HO_2^\bullet$ reaction.

An additional unresolved question concerns the electronic state of the CH_3OOOOH adduct. When a $CH_3O_2^\bullet$ and a $HO_2^\bullet$ in their electronic ground state ($^2A''$) react, the spin state of the overall system they form can be either a singlet spin state or a triplet one. However, if one assumes that the products of reaction eq 4 are formed in their electronic ground state, namely, singlet CH_3OOH (^1A) plus $^3O_2$, then these products can only be reached on the triplet potential energy surface (PES). There arises the question of whether (a) CH_3OOOOH is a bound-triplet-state species, which may be possible for a hydrogen-bonded species where the unpaired electrons would not be required for bonding, or (b) the formed products are ground-state singlet CH_3OOH and excited singlet molecular oxygen (O_2, $^1\Delta_g$), designated by $^1O_2$. To elucidate the mechanism by which CH_3OOH is formed and ascertain the spin multiplicity of the transition state involved, there is need for rigorous quantum-chemical calculations of the singlet and triplet PESs of the $CH_3O_2^\bullet + HO_2^\bullet$ reaction.

Recently, Hou and Wang have reported the first theoretical calculations on the reactions of $HO_2^\bullet$ with $CH_3O_2^\bullet$ and $CH_2FO_2^\bullet$.[8] Using various ab initio methods, including MP2, CISD, QCISD(T), and CCSD(T), as well as density functional theory (B3LYP), both singlet and triplet PESs were investigated. On the basis of CCSD(T)/cc-pVDZ energy calculations performed at the B3LYP/6-311G(d,p)-optimized geometries of stationary points (minima and saddle points) located on the PESs, Hou and Wang conclude that the $CH_3O_2^\bullet + HO_2^\bullet$ reaction proceeds only on the triplet PES through hydrogen abstraction and that CH_3OOH is the dominant product, while the reaction paths on the singlet PES cannot be competitive because of significant barriers. Taking into account the expected multireference character of the wave function of various stationary points on the singlet PES, the predictions based on single-determinant B3LYP and single-reference CCSD(T) calculations are at least questionable.

We feel that the conclusions drawn from the theoretical calculations of Hou and Wang concerning the reaction pathways on the singlet PES of the reactions of $HO_2^\bullet$ with $CH_3O_2^\bullet$ merit further study. With this purpose, here we report the results of multireference second-order perturbative energy calculations CASPT2/6-311+G(3df,2p) carried out on the CASSCF/6-311+G(3df,2p) geometries pertaining to the reaction pathways explored on both the singlet and triplet PESs of the $CH_3O_2^\bullet + HO_2^\bullet$ reaction, in a continued effort to elucidate the mechanism of this important reaction.

2. Computational Methods

The geometries of the relevant stationary points on both the singlet and triplet PESs of the $CH_3O_2^\bullet + HO_2^\bullet$ reaction system were optimized by use of multiconfiguration self-consistent field (MCSCF) wave functions of the complete active space (CAS) SCF class[9] with the triple split-valence 6-311+G(3df,2p) basis set[10] (which includes a single diffuse sp shell,[11] triple d-polarization, and a single additional f-polarization on heavy atoms and double p-polarization on hydrogen atoms) employing analytical gradient procedures.[12,13] The CAS of each stationary point was selected following the procedure suggested by Anglada and Bofill,[14] based on the fractional occupation of the natural orbitals generated from the first-order density matrix calculated from an initial multireference single- and double-excitation configuration interaction (MRDCI) wave function correlating all valence electrons. The CAS varied from four electrons in four molecular orbitals (MOs), labeled as (4,4), for CH_3OOH to twelve electrons in ten MOs, labeled as (12,10), for several stationary points. Thus, for $CH_3O_2^\bullet$ the fractional occupancies of the natural orbitals indicated that there are seven electrons in six MOs, labeled as (7,6), namely, the σ, σ^* orbitals of the CO fragment and the σ, σ^* and π, π^* orbitals of the OO fragment, whereas for $HO_2^\bullet$ the fractional occupancies of the natural orbitals indicated that there are five electrons in four MOs, labeled as (5,4), namely, the σ, σ^* and π, π^* orbitals of the OO fragment. In the case of the products, the CAS of CH_3OOH comprised the σ, σ^* orbitals of the CO fragment and the σ, σ^* orbitals of the OO fragment, whereas the CAS of O_2 comprised eight electrons in six MOs, labeled as (8,6), which included the σ_z, σ_z^* and π_x, π_x^* and π_y, π_y^* orbitals of the OO bond.

All the stationary points were characterized by their harmonic vibrational frequencies as minima or saddle points. The harmonic vibrational frequencies were obtained by diagonalizing the mass-weighted Cartesian force constant matrix calculated at the CASSCF/6-311+G(3df,2p) level. Connections of the transition structures between designated minima were confirmed in each case by IRC calculations[15] at the latter level of theory using the second-order algorithm of Gonzalez and Schlegel.[16] All CASSCF calculations were carried out by using the GAMESS system of programs.[17]

To incorporate the effect of dynamical valence-electron correlation on the relative energy ordering of the stationary points, second-order multiconfigurational perturbation theory calculations based on the CASSCF(12,10) reference function (CASPT2)[18] were carried out with the 6-311+G(3df,2p) basis set. CASPT2/6-311+G(3df,2p) single point energies were calculated at the geometries optimized at the CASSCF/6-311+G(3df,2p) level, and all valence electrons were correlated. Since the "normal" CASPT2 method, sometimes denoted as CASPT2-0, is known to underestimate the energy of some open-shell relative to closed-shell electronic states, the CASPT2-g1 procedure with the full Hartree−Fock matrix was used in the construction of the zeroth-order Hamiltonian.[19] Moreover, for the hydrogen-bonded complexes found in this work, the basis set superposition error (BSSE) was calculated at the CASPT2/6-311+G(3df,2p) level by using the counterpoise method of Boys and Bernardi.[20] The CASPT2 computations were performed with the MOLCAS 5 program pakage.[21]

Zero-point vibrational energies (ZPVEs) were determined from unscaled harmonic vibrational frequencies. Absolute entropies and thermal corrections to enthalpy and Gibbs free-energy values were obtained assuming ideal gas behavior from the unscaled harmonic frequencies and moments of inertia by standard methods.[22] A standard pressure of 1 atm was taken in the absolute entropy calculations.

To examine the characteristics of the bonding and interactions in the most relevant structures we have also performed an

analysis of the electronic charge density within the framework of the topological theory of atom in molecules (AIM) making use of the PROAIM and EXTREME programs of Bader et al.[23] The first-order electron density matrix obtained from the CASSCF/6-311+G(3df,2p) wave function was used in this analysis. The theory of AIM has been reviewed in the literature and in a monograph.[24] For the convenience of the reader, we will summarize some important points here. The topological characteristics of the electronic charge density, $\rho(\mathbf{r})$ ($\mathbf{r} \in x,y,z$), give rise to a rigorous partitioning of the real space comprising a molecule into different atomic basins. In AIM theory, an atom consists of a nucleus and its associated atomic basin. Properties such as charges, dipole, and quadrupole moments can thus unequivocally be assigned to individual atoms by integration of the desired property over their atomic basin. Chemical bonds between pairs of atoms can be identified by (3,−1) critical points (also called "bond critical points") of the electronic charge density $\rho(\mathbf{r})$. At such points $\mathbf{r}_b$ the gradient vector of $\rho(\mathbf{r})$ vanishes. The notation (3,−1) implies that, in addition, the Hessian matrix of $\rho(\mathbf{r})$ at $\mathbf{r}_b$ has three nonvanishing eigenvalues, two of which are negative and one positive. The line of maximum charge density linking the nuclei of the pairs of atoms passes through $\mathbf{r}_b$. This line is called a bond path. The charge density at the bond critical point, $\rho(\mathbf{r}_b)$, provides a measure for the covalent bond order between a given pair of atoms. Furthermore, the value of the Laplacian of $\rho(\mathbf{r})$ at the bond critical point, $\nabla^2\rho(\mathbf{r}_b)$, i.e., the sum of the three eigenvalues of Hessian matrix, indicates whether covalent or closed-shell interactions prevail between the two bonded atoms. $\nabla^2\rho(\mathbf{r})$ identifies regions of space wherein $\rho(\mathbf{r})$ is locally concentrated ($\nabla^2\rho(\mathbf{r}) < 0$) or depleted ($\nabla^2\rho(\mathbf{r}) > 0$). Therefore, a negative value of $\nabla^2\rho(\mathbf{r})$ in the internuclear region of two interacting atoms implies the formation of a covalent bond, since electron density is built up in that region, while positive values are characteristic of closed-shell interactions, such as ionic, van der Waals, and hydrogen bonding, where the electron density is depleted from the internuclear region and concentrated on the corresponding atomic basins. Useful information is also related to (3,+1) critical points of the electron density (also called "ring critical points"). The notation (3,+1) implies that the Hessian matrix of $\rho(\mathbf{r})$ at such points $\mathbf{r}_r$ has three nonvanishing eigenvalues, two of which are positive. A ring critical point occurs as consequence of the fact that some bond paths are linked so as to form a ring of bonded atoms. Then a ring critical point is found in the interior of the ring.

3. Results and Discussion

The Cartesian coordinates of all structures reported in this article are available as Supporting Information. Total electronic energies computed at the CASSCF and CASPT2 levels of theory with the 6-311+G(3df,2p) basis set, as well as the ZPVEs, absolute entropies, and thermal corrections to enthalpy and Gibbs free energy, are collected in Table S1 (Supporting Information). For all stationary points, Table 1 gives the relative electronic energies (ΔU), the relative energies including the ZPVE correction (ΔE(0 K)), and the relative enthalpies (ΔH(298 K)) and Gibbs free energies (ΔG(298 K)) at 298 K, calculated at the CASPT2/6-311+G(3df,dp) level.

3.1. Reactants and Products. Selected geometrical parameters of the reactants $CH_3O_2^\bullet$ and $HO_2^\bullet$ (labeled as **1** and **2**, respectively) and products CH_3OOH, $^1O_2$, and $^3O_2$ (labeled as **3**, $^1\mathbf{O_2}$, and $^3\mathbf{O_2}$, respectively) of reaction eq 4 are shown in Figure 1. It is worth noting that the geometries calculated for $CH_3O_2^\bullet$ and $HO_2^\bullet$ compare well with previous results in the literature.[25−39] Thus, the values of the most relevant geometrical parameters of **1** (C1−O1 = 1.456 Å, O1−O2 = 1.336 Å, and C1−O1−O2 = 109.2°) agree reasonably well with those (C1−O1 = 1.443 Å, O1−O2 = 1.325 Å, and C1−O1−O2 = 110.3°) calculated by Aplincourt et al.[35] for $CH_3O_2^\bullet$ at the QCISD/6-311++G(d,p) level, which appears to be the best ab initio calculation reported for this molecule. The geometry of **2** (O1−O2 = 1.350 Å, H1−O2 = 0.947 Å, and H1−O2−O1 = 104.1°) also agrees reasonably well with that (O1−O2 = 1.335 Å, H1−O2 = 0.971 Å, and H1−O2−O1 = 104.4°) calculated by Francisco and Zhao for $HO_2^\bullet$ at the QCISD(T)/6-311G(d,p) level,[30] which is in remarkable agreement with the experimental geometry (O1−O2 = 1.331 Å, H1−O2 = 0.971 Å, and H1−O2−O1 = 104.1°) reported by Lubic and Amano.[40] Concerning the geometry of **3**, the values of the most relevant geometrical parameters (O1−O2 = 1.471 Å, C1−O1 = 1.433 Å, H1−O2 = 0.943 Å, C1−O1−O2 = 105.1°, and H1−O2−O1 = 100.0°) compare reasonably well with those (O1−O2 = 1.468 Å, C1−O1 = 1.419 Å. H1−O2 = 0.967 Å, C1−O1−O2 = 104.5°, and H1−O2−O1 = 98.4°) calculated by Wallington et al.[41] for

TABLE 1: Relative Energies (kcal/mol) of the Most Relevant Stationary Points on the Lowest Singlet and Triplet State Potential Energy Surfaces for the $CH_3O_2^\bullet + HO_2^\bullet$ Reaction System[a]

stationary point[b]	ΔU[c]	ΔE(0 K)[d]	ΔH(298 K)	ΔG(298 K)
1 + 2	0.0	0.0	0.0	0.0
CX-S	−5.8 (−6.4)	−4.9 (−5.5)	−4.6 (−5.2)	3.5 (2.9)
TS1-S	6.6	5.5	4.4	17.1
TS1′-S	14.0	11.9	11.3	22.4
3 + $^1O_2$	−13.1	−12.6	−12.6	−11.2
TS2-S	−3.6	−1.8	−2.6	9.2
4	−9.1	−6.4	−7.4	5.0
TS3-S	39.5	38.2	37.3	49.3
TS4-S	20.4	18.7	17.6	30.4
CX-T	−5.6 (−6.2)	−4.5 (−5.1)	−4.4 (−5.0)	3.6 (3.0)
TS1-T	−1.1	−3.8	−4.4	6.3
TS1′-T	1.4	−1.5	−2.0	8.0
3 + $^3O_2$	−37.5	−36.9	−36.9	−35.5

[a] Calculated at the CASPT2/6-311+G(3df,2p) level of theory including the BSSE correction for **CX-S** and **CX-T** hydrogen-bonded complexes. The values given in parentheses do not include the BSSE correction. [b] See Figures 2 and 8. [c] Relative electronic energies. [d] Relative energies including the ZPVE correction.

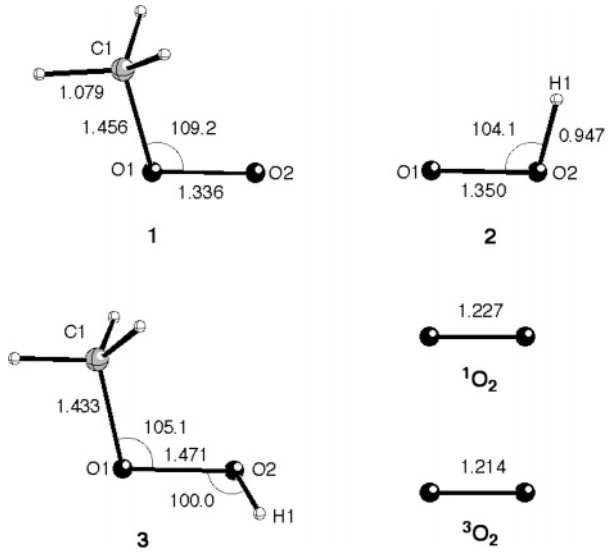

Figure 1. Selected geometrical parameters of the CASSCF/6-311+G(3df,2p)-optimized geometries of the reactants and products of the $CH_3O_2^\bullet + HO_2^\bullet$ reaction. Distances are given in Å and angles in deg.

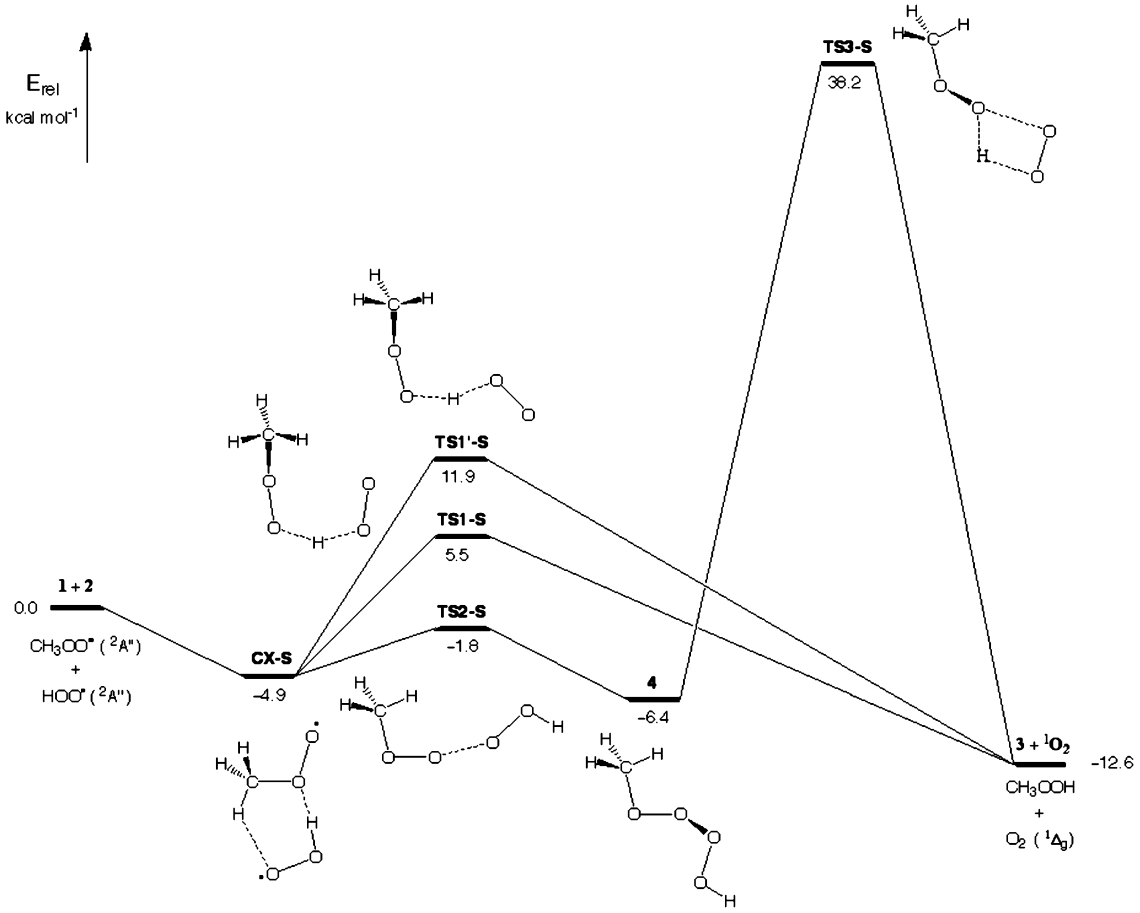

Figure 2. Schematic energy profiles along an arbitrary reaction coordinate showing the stationary points involved in the reaction pathways on the singlet PES leading to $CH_3OOH + {}^1O_2$. Relative energy values obtained from the ZPVE-corrected CASPT2/6-311+G(3df,2p) total energies.

CH_3OOH at the MP2/6-31G(d,p) level. Finally, we note that the O−O bond lengths of 1.227 and 1.214 Å of $^1\mathbf{O_2}$ and $^3\mathbf{O_2}$, respectively, are in good agreement with the experimental values of 1.22 and 1.21 Å.[42]

3.2. The Singlet Potential Energy Surface. Figure 2 displays schematic energy profiles showing the most relevant stationary points concerning the reaction pathways on the singlet PES leading to $\mathbf{3} + {}^1\mathbf{O_2}$. The relative energy values were obtained from ZPVE-corrected CASPT2/6-311+G(3df,2p) total energies calculated at the CASSCF/6-311+G(3df,2p)-optimized geometries (see ΔE(0 K) in Table 1).

3.2.1. Prereactive Hydrogen-Bonded Complex. As it is not uncommon in many gas-phase reactions of interest in atmospheric chemistry, the reaction between $CH_3O_2^\bullet$ and $HO_2^\bullet$ on the singlet PES begins with the barrierless formation of a prereactive loosely bound complex in the entrance channel, labeled as **CX-S** (see Figure 3). The optimized structure of **CX-S** has C_s symmetry and was characterized as a true local minimum on the PES. As compared with the bond distances in **1** and **2**, **CX-S** shows a 0.026 Å lengthening of the H1−O4 distance (see Figure 3 for atom numbering) and a 0.035 Å shortening of the C1−O1 bond. Interestingly enough, the AIM topological analysis of the electron charge density in **CX-S** revealed the presence of a bond critical point between the atoms O1 and H1 and of another bond critical point between the atoms O3 and H2, indicating that there is a bonding interaction between these atom pairs. The low value of the electron charge density at the bond critical point (i.e., $\rho(\mathbf{r}) = 0.0141$ and 0.0033 e bohr^{-3}, for the H1···O1 and O3···H2 atom pairs, respectively) and the positive value of the Laplacian (i.e., $\nabla^2\rho(\mathbf{r}) = 0.0627$ and 0.0133 e bohr^{-5}, for the H1···O1 and O3···H2 atom pairs,

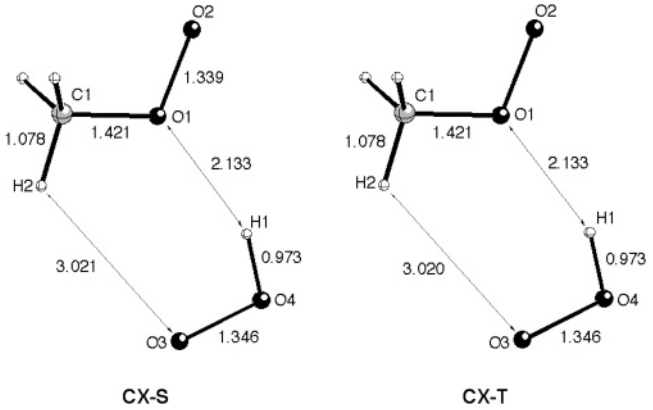

Figure 3. Selected geometrical parameters of the CASSCF/6-311+G(3df,2p)-optimized geometries of the singlet (**CX-S**) and triplet (**CX-T**) hydrogen-bonded complexes. Distances are given in Å.

respectively) calculated for these bond critical points are typically associated with hydrogen-bond-like interactions. In addition, a ring critical point with a small electron charge density ($\rho(\mathbf{r}) = 0.0300$ e bohr^{-3}) was located in the middle of the six-membered ring formed by the O1, C1, H2, O3, O4, and H1 atoms. These electronic features indicate the formation of two hydrogen bonds between the CH_3O_2 and HO_2 moieties of **CX-S**, which leads to a six-membered-ring equilibrium structure with two abnormally long H···O intermolecular distances (i.e., H1···O1 = 2.133 Å and H2···O3 = 3.021 Å). At the CASPT2 level of theory, **CX-S** lies 6.4 kcal/mol below the energy of the isolated reactants **1** plus **2**. Inclusion of the correction for the BSSE leads to a stabilization energy of **CX-S** toward decomposition into **1** and **2** of 5.8 kcal/mol. Inclusion of the ZPVE

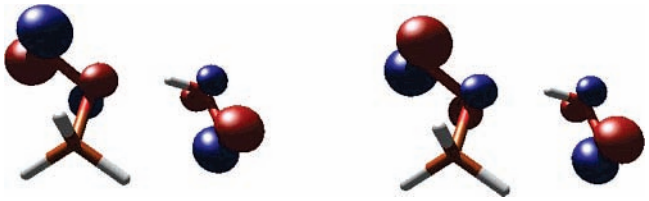

Figure 4. Representation of the natural orbitals with electron occupations of 1.022 (left) and 1.017 (right) in the hydrogen-bonded singlet diradical complex **CX-S**.

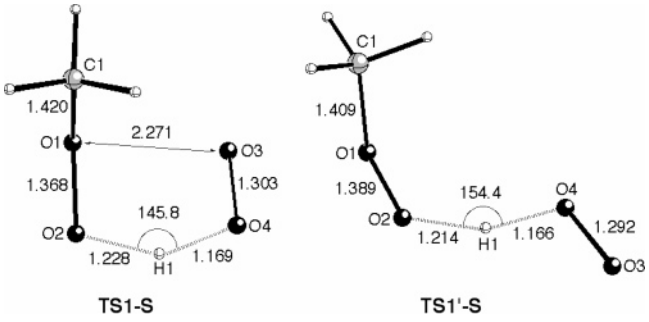

Figure 5. Selected geometrical parameters of the CASSCF/6-311+G(3df,2p)-optimized geometries of the transition structures for direct H-atom transfer from $HO_2^{\bullet}$ to $CH_3O_2^{\bullet}$ on the singlet PES. Distances are given in Å and angles in deg.

correction to the latter value gives a stabilization energy of 4.9 kcal/mol at 0 K.

An inspection of the CASSCF(12,10) natural orbitals obtained for **CX-S** revealed the presence of two orbitals of a″ symmetry with electron occupancies of 1.022 and 1.017, which are shown in Figure 4. Basically, these singly occupied orbitals are the positive and negative combinations of the π-type orbitals describing the unpaired electron of the isolated radicals **1** and **2**. Therefore, **CX-S** is a hydrogen-bonded species where the unpaired electrons of the two radical moieties are not used for bonding but are coupled to an overall open-shell singlet of A′ symmetry. It is to be mentioned that no hydrogen-bonded complex on the singlet PES was found at the B3LYP level of theory in the recent study of Hou and Wang.[8] In this regard, we note that single-reference-based methods, including B3LYP, MP2, CISD, QCISD(T), and CCSD(T), become inadequate to deal with open-shell singlet species such as **CX-S**.

3.2.2. Direct H-Atom Transfer. We have found two transition structures, labeled as **TS1-S** and **TS1′-S** (see Figure 5), for direct H-atom transfer between the HO_2 and CH_3O_2 moieties of **CX-S** on the singlet PES. These transition structures differ one from the other essentially in the orientation of the O3−O4 bond of the HO_2 moiety with respect to the O1−O2 bond of the CH_3O_2 moiety, **TS1-S** with both bonds in a *cisoid* position, and **TS1′-S** with both bonds in a *transoid* position. In both transition structures the O2−H1−O4 angle deviates significantly from the "optimum" value of 180° expected for an intermolecular H-atom transfer.[43] Hou and Wang[8] have located at the B3LYP/6-311G(d,p) level a single transition structure (referred a TS3) for the direct H-atom transfer from $HO_2^{\bullet}$ to $CH_3O_2^{\bullet}$ on the singlet PES. This transition structure shows a *transoid* conformation similar to that of **TS1′-S**, but the distances of the O−H breaking and forming bonds (1.000 and 1.630 Å) differ significantly from our values (1.166 and 1.214 Å).

At the CASPT2 level of theory **TS1-S** is calculated to be 7.4 kcal/mol less energetic than **TS1′-S** (see ΔU values in Table 1). On the basis that the O1−O3 distance in **TS1-S** (2.271 Å) is 0.529 Å shorter than twice the oxygen atom van der Waals nonbonded radius (1.40 Å),[44] one would expect **TS1-S** to be higher in energy than **TS1′-S** owing to the electrostatic repulsion between the lone pairs of the O1 and O3 atoms in **TS1-S**. What is the origin of the lower energy found for **TS1-S** as compared with that of **TS1′-S**? At this point it is worth noting that the AIM analysis of the electron density in **TS1-S** revealed the presence of a bond critical point between the atoms O1 and O3, indicating that there is a bonding interaction between this atom pair. The small electron charge density ($\rho(\mathbf{r}) = 0.0359$ e bohr^{-3}) and the positive value of the Laplacian ($\nabla^2\rho(\mathbf{r}) = 0.1591$ e bohr^{-5}) calculated for this bond critical point suggest that O1 and O3 are weakly bonded by an intermolecular noncovalent O···O interaction. Although unusual, this kind of interaction has been found in other species[45−49] and its origin has been analyzed elsewhere.[46] Consequently, the lower energy of **TS1-S** with respect to **TS1′-S** can be ascribed to an intermolecular noncovalent bonding interaction between the O1 and O3 atoms, which is lacking in **TS1′-S** due to the long distance between these atoms. It is worth noting that at the CASSCF level of theory the energy difference between **TS1-S** and **TS1′-S** is 5.5 kcal/mol (see Table S1, Supporting Information), whereas at the CASPT2 level this energy difference rises to 7.4 kcal/mol. Therefore, the dynamic valence-electron correlation plays an important role in the aforementioned intermolecular noncovalent O···O interaction.

The IRC calculations showed that both **TS1-S** and **TS1′-S** go backward to the hydrogen-bonded complex **CX-S** and go forward to give the products **3** plus $^1\mathbf{O_2}$. According to Table 1, the H-atom transfer from **2** to **1** on the singlet PES leading to the formation of these products is predicted to involve an energy of reaction of −12.6 kcal/mol at 0 K. Inclusion of the thermal correction to enthalpy leads to the same value for the enthalpy of reaction at 298 K (ΔH_r(298 K)). Although the experimental value for this reaction is unknown, an estimate of −15.5 kcal/mol can be obtained from the ΔH_r(298 K) of −38.0 kcal/mol determined[6] for the H-atom transfer from $HO_2^{\bullet}$ to $CH_3O_2^{\bullet}$ yielding CH_3OOH plus $^3O_2$ and the experimental $^3O_2-^1O_2$ energy gap of 22.5 kcal/mol.[42]

The direct H-atom transfer from **2** to **1** on the singlet PES through the lowest energy transition structure **TS1-S** involves a 0 K activation energy ($\Delta E^{\ddagger}$(0 K)) of 5.5 kcal/mol. We note that this activation energy is much lower than that (9.31 kcal/mol) obtained from the ZPVE-corrected CCSD(T)/cc-pVDZ//B3LYP/6-311G(d,p) energies reported by Hou and Wang.[8] This discrepancy is mainly ascribed to the fact that the transition structure found by the latter authors (referred as TS3) possesses a *transoid* orientation of the O1−O2 and O3−O4 bonds, which prevents the aforementioned intermolecular noncovalent O··· O interaction.

3.2.3. Stepwise Mechanism. The adduct CH_3OOOOH was indeed found to be a minimum on the ground-state singlet PES. The lowest energy conformer of such a tetraoxide, labeled as **4**, is shown in Figure 6. The main geometrical findings for **4** are that the intraradical O−O bond distances show an increase of 0.078 (O1−O2) and 0.093 (O3−O4) Å when going from the isolated reactants **1** and **2** to the tetraoxide **4** and the significant long distance (1.461 Å) of the newly formed O2−O3 bond. The latter feature suggests that the addition (recombination) between the terminal oxygen atoms of radicals $CH_3O_2^{\bullet}$ and $HO_2^{\bullet}$ leads to the formation of a rather weak O−O single bond. While the experimental ΔH_r(298 K) of this reaction is unknown, our calculations (see Table 1) predict a ΔH_r(298 K) of only −7.4 kcal/mol, which is consistent with the predicted long O2−O3 bond distance.

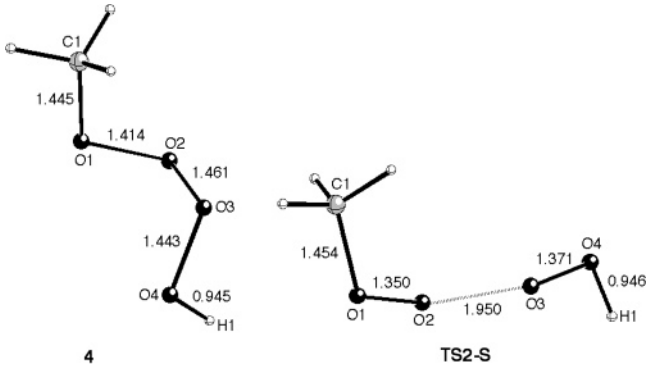

Figure 6. Selected geometrical parameters of the CASSCF/6-311+G-(3df,2p)-optimized geometries of the tetraoxide intermediate (**4**) and the transition structure (**TS2-S**) for the addition of $HO_2^{\bullet}$ to $CH_3O_2^{\bullet}$ on the singlet PES. Distances are given in Å.

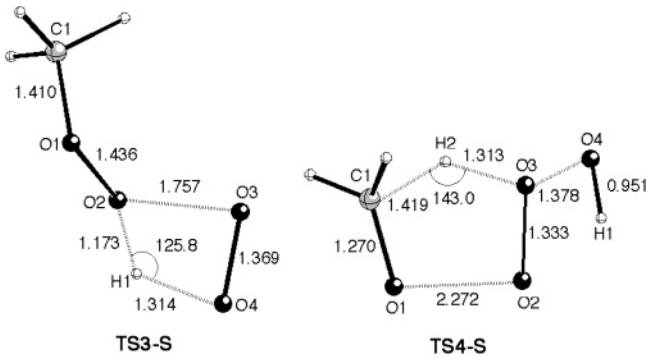

Figure 7. Selected geometrical parameters of the CASSCF/6-311+G-(3df,2p)-optimized geometries of the transition structures for the rearrangement of **4** yielding $CH_3OOH + {}^1O_2$ (**TS3-S**) and $CH_2O + HO_2^{\bullet} + HO^{\bullet}$ (**TS4-S**) on the singlet PES. Distances are given in Å and angles in deg.

At this point we note that the first step of the addition of **1** to **2** leading to **4** is the formation of the hydrogen-bonded complex **CX-S** without surmounting an energy barrier (see Figure 2). The second step is the formation of a single bond between the oxygen atoms O2 and O3 in **CX-S**, which involves the passage through a transition structure, labeled as **TS2-S**, whose optimized geometry is shown in Figure 6. As expected for the transition structure of a reaction involving the addition of two radicals (or the homolytic dissociation of the corresponding adduct), the wave function of **TS2-S** displays a large amount of multireference character. In fact, an inspection of the CASSCF(12,10) natural orbitals obtained for **TS2-S** revealed the presence of two orbitals with electron occupancies of 1.6181 and 0.4122, which are the positive and negative combinations of the π-type orbitals describing the unpaired electrons of the CH_3O_2 and HO_2 components. Although the energy of **TS2-S** is calculated to be lower than that of the isolated reactants **1** plus **2**, the formation of **4** from **CX-S** involves a $\Delta E^{\ddagger}(0\ \mathrm{K})$ of 3.1 kcal/mol. These findings are in clear contrast with the results of the B3LYP/6-311G(d,p) calculations by Hou and Wang[8] predicting the barrierless direct formation of the tetraoxide adduct from the $CH_3O_2^{\bullet}$ and $HO_2^{\bullet}$ radicals.

The subsequent rearrangement of **4** yielding **3** plus $^1\mathbf{O_2}$ takes place through a strained four-membered-ring transition structure, labeled as **TS3-S** (Figure 7), in which the CH_3O group does not participate itself. It is worth noting that this transition structure involves the concerted breaking of two bonds (i.e., O2−O3 and H1−O4) and forming of a bond (i.e., O2−H1). As expected for such a strained structure, **TS3-S** is calculated to lie high in energy above the tetraoxide **4**. In fact, the rearrangement of this intermediate yielding **3** plus $^1\mathbf{O_2}$ is predicted to involve a $\Delta E^{\ddagger}(0\ \mathrm{K})$ of 44.6 kcal/mol (see Table 1), which is significantly lower than the value of 50.78 kcal/mol obtained from the ZPVE-corrected CCSD(T)/cc-pVDZ//B3LYP/6-311G(d,p) energies reported by Hou and Wang.[8] It is likely that this discrepancy is due is to the multireference character of **TS3-S** arising from the fact that this transition structure connects the closed-shell intermediate **4** with the $^1\Delta_g$ open-shell singlet state of oxygen $^1O_2$.

Although our investigation focused on the mechanism of reaction eq 4, for the sake of completeness we also calculated the transition structure, labeled as **TS4-S** (Figure 7), for the rearrangement of tetraoxide **4** giving CH_2O, $HO_2^{\bullet}$, and $HO^{\bullet}$. This reaction channel yielding a carbonyl compound has been found to be unimportant for unsubstituted alkylperoxy radicals. However, in the case of halogenated alkylperoxy radicals (e.g., $CH_2FO_2^{\bullet}$, $CH_2ClO_2^{\bullet}$, $CHCl_2O_2^{\bullet}$, etc.) the formation of the corresponding halogenated carbonyl compound (e.g., CHFO, CHClO, CCl_2O, etc.) appears to be dominant.[41,50,51] We note that **TS4-S** contains a five-membered ring and involves the concerted breaking of three bonds (i.e., O1−O2, O3−O4, and H2−C1) and forming of a bond (i.e., O3−H2). As a result of this energetically unfavorable process, **TS4-S** is calculated to lie high in energy above the tetraoxide **4**. Thus, the rearrangement of this intermediate yielding CH_2O, $HO_2^{\bullet}$, and $HO^{\bullet}$ is calculated to involve a $\Delta E^{\ddagger}(0\ \mathrm{K})$ of 18.7 kcal/mol (see Table 1), which is significantly larger than the value of 10.3 kcal/mol obtained from the ZPVE-corrected CCSD(T)/cc-pVDZ//B3LYP/6-311G(d,p) energies reported by Hou and Wang.[8] As expected for the transition structure of a reaction leading to the formation of two radical species (i.e., $HO_2^{\bullet}$ and $HO^{\bullet}$) from a closed-shell reactant, the wave function of **TS4-S** is found to show a significant degree of multireference character. Therefore, the predictions concerning the relative energy of this transition structure based on single-reference CCSD(T) calculations are questionable.

In summary, the present calculations indicate that the currently accepted stepwise mechanism "A" (Scheme 1) on the singlet PES is predicted to be energetically very unfavorable, as compared with the direct H-atom-transfer mechanism "B". Moreover, the alternative reaction channel leading to the formation of CH_2O from the rearrangement of the tetraoxide intermediate cannot compete with the direct H-atom transfer, either, because it involves a large energy barrier.

3.3. The Triplet Potential Energy Surface. Figure 8 displays schematic energy profiles showing the most relevant stationary points concerning the reaction pathways on the triplet PES leading to **3** plus $^3\mathbf{O_2}$. The relative energy values were obtained from ZPVE-corrected CASPT2/6-311+G(3df,2p) total energies calculated at the CASSCF/6-311+G(3df,2p)-optimized geometries (see $\Delta E(0\ \mathrm{K})$ in Table 1).

3.3.1. Prereactive Hydrogen-Bonded Complex. The reaction between $CH_3O_2^{\bullet}$ and $HO_2^{\bullet}$ on the triplet PES begins with the barrierless formation of a prereactive loosely bound complex in the entrance channel, labeled as **CX-T** (see Figure 3), which was characterized as a true local minimum. The optimized geometry of **CX-T** has C_s symmetry and is nearly identical to that of **CX-S**. The AIM topological analysis of the electron charge density in **CX-T** also revealed the presence of a bond critical point between the atoms O1 and H1 and of another bond critical point between the atoms O3 and H2, indicating the formation of two hydrogen bonds between the CH_3O_2 and HO_2 moieties of **CX-T**, which leads to a six-membered-ring equilibrium structure with two abnormally long H···O intermolecular

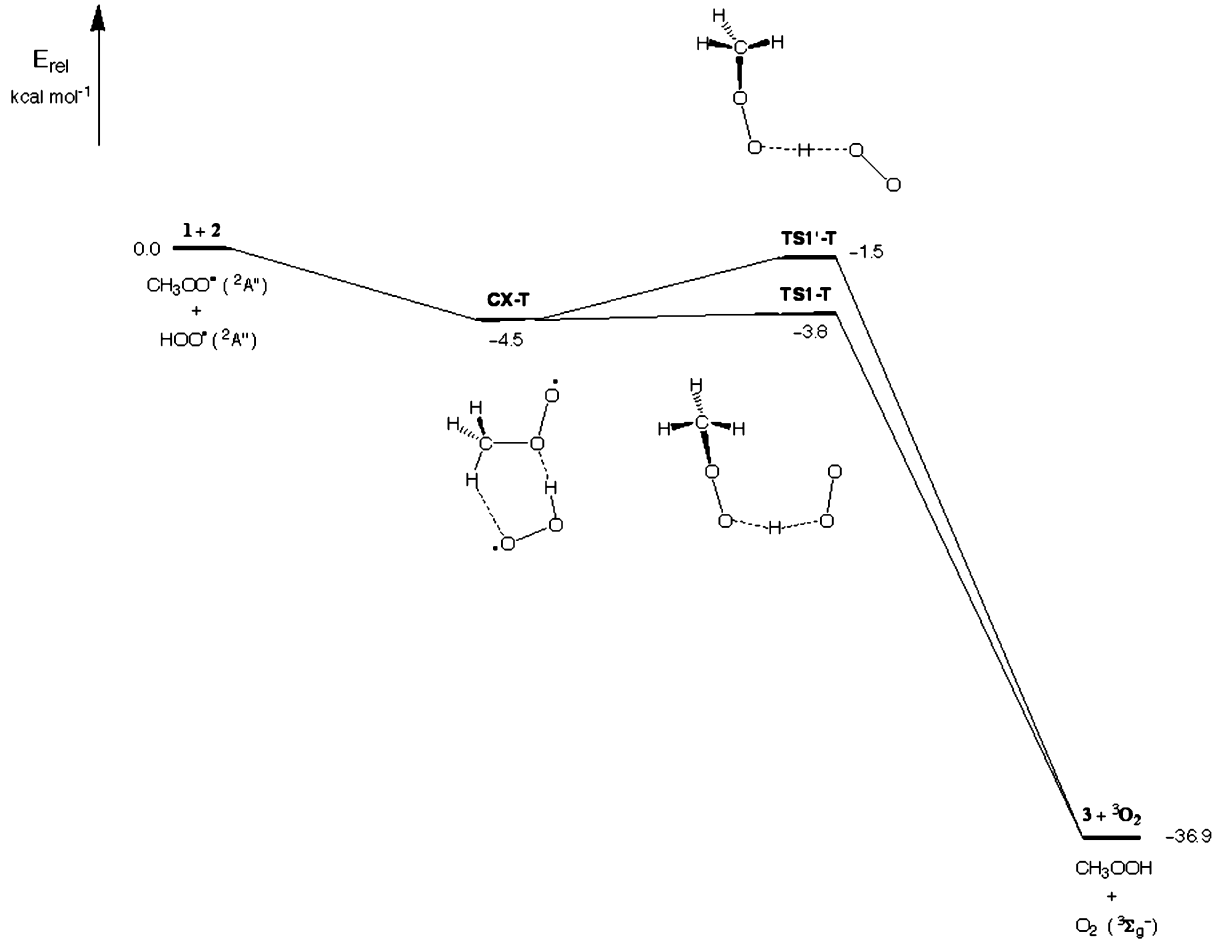

Figure 8. Schematic energy profiles along an arbitrary reaction coordinate showing the stationary points involved in the reaction pathways on the triplet PES leading to $CH_3OOH + {}^3O_2$. Relative energy values obtained from the ZPVE-corrected CASPT2/6-311+G(3df,2p) total energies.

distances (i.e., H1···O1 = 2.133 Å and H2···O3 = 3.020 Å). An analysis of the CASSCF(12,10) natural orbitals calculated for **CX-T** indicated the presence of two orbitals of a″ symmetry with electron occupancies of 1.0195 and 1.0193, which are nearly identical to the natural orbitals of **CX-S** shown in Figure 3. Therefore, **CX-T** is a hydrogen-bonded species where the unpaired electrons of the two radical moieties are not employed for bonding but are coupled to an overall triplet of A′ symmetry. It is to be noted that, at variance with the open-shell singlet **CX-S**, the single-reference based methods such as UB3LYP can give a reasonable description of the hydrogen-bonded triplet complex **CX-T**. In this connection it is worth mentioning that the geometry of the hydrogen-bonded complex located at the UB3LP/6-311G(d,p) level on the triplet PES by Hou and Wang[8] is qualitatively similar to that calculated for **CX-T**.

At the CASPT2 level, **CX-T** lies 6.2 kcal/mol below the energy of the isolated reactants **1** plus **2**. Inclusion of the correction for the BSSE leads to a stabilization energy of **CX-T** toward decomposition into **1** and **2** of 5.6 kcal/mol. On the basis of the ΔU values given in Table 1, the hydrogen-bonded complexes **CX-S** and **CX-T** are essentially degenerate and, therefore, correspond to the singlet and triplet states of a diradical species. Inclusion of the ZPVE correction to the relative energy of **CX-T** with respect to the reactants **1** and **2** gives a stabilization energy of 4.5 kcal/mol at 0 K, which is only 0.4 kcal/mol lower than that calculated for **CX-S**.

3.3.2. Direct H-Atom Transfer. As in the case of the singlet PES, two transition structures, labeled as **TS1-T** and **TS1′-T** (see Figure 9), have been found for direct H-atom transfer between the HO_2 and CH_3O_2 moieties of **CX-T**. Again, these

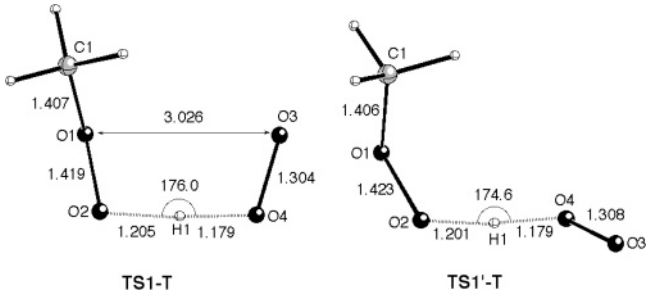

Figure 9. Selected geometrical parameters of the CASSCF/6-311+G-(3df,2p)-optimized geometries of the transition structures for direct H-atom transfer from $HO_2^{\bullet}$ to $CH_3O_2^{\bullet}$ on the triplet PES. Distances are given in Å and angles in deg.

transition structures differ one from the other essentially in the orientation of the O3−O4 bond of the HO_2 moiety with respect to the O1−O2 bond of the CH_3O_2 moiety, **TS1-T** with both bonds in a *cisoid* position, and **TS1′-T** with both bonds in a *transoid* position. We note that the O2−H1−O4 angle in **TS1-T** (176.0°) and **TS1′-T** (174.6°) is closer to the "optimum" expected value of 180° than in the case of both **TS1-S** (145.8°) and **TS1-S** (154.4°). Hou and Wang[8] have found at the UB3LYP/6-311G(d,p) level a single transition structure (referred as TS1) for the direct H-atom transfer between the HO_2 and CH_3O_2 partners of a hydrogen-bonded complex on the triplet PES. This transition structure shows a *cisoid* conformation similar to that of **TS1-T**, but the distances of the O−H breaking and forming bonds (1.030 and 1.509 Å) differ significantly from the values (1.179 and 1.205 Å) calculated for **TS1-T**.

TABLE 2: Equilibrium Constant (K_{eq} in molecule^{-1} cm^3; See Eq 7) of the First Step, Tunneling Factor (Γ) and Rate Constant (k_2 in molecule^{-1} cm^3 s^{-1}; See Eq 8) of the Second Step, and Rate Constant (k_{RP} in molecule^{-1} cm^3 s^{-1}; See Eq 6) for Five Reaction Pathways Located on the Singlet and Triplet Potential Energy Surfaces of the $CH_3O_2^\bullet + HO_2^\bullet$ Reaction System

	225 K	250 K	275 K	300 K	325 K	350 K	375 K
			Singlet Reaction Pathways				
K_{eq}	1.12×10^{-21}	4.26×10^{-22}	1.97×10^{-22}	1.06×10^{-22}	6.35×10^{-23}	4.16×10^{-23}	2.92×10^{-23}
TS1-S							
Γ	3.56x 10^5	4.15×10^4	7.59×10^3	1.95×10^3	6.47×10^2	2.64×10^2	1.26×10^2
k_2	3.05×10^5	3.55×10^5	4.22×10^5	5.12×10^5	6.33×10^5	7.91×10^5	1.00×10^6
k_{RP}	3.42×10^{-16}	1.51×10^{-16}	8.31×10^{-17}	5.41×10^{-17}	4.01×10^{-17}	3.29×10^{-17}	2.92×10^{-17}
TS1′-S							
Γ	3.29x 10^{13}	7.47×10^{11}	3.43×10^{10}	2.66×10^9	3.10×10^8	4.97×10^7	1.03×10^7
k_2	9.51×10^7	9.98×10^7	1.05×10^8	1.11×10^8	1.17×10^8	1.24×10^8	1.32×10^8
k_{RP}	1.07×10^{-13}	4.25×10^{-14}	2.07×10^{-14}	1.17×10^{-14}	7.44×10^{-15}	5.17×10^{-15}	3.86×10^{-15}
TS2-S							
Γ	1.04	1.03	1.03	1.02	1.02	1.02	1.02
k_2	3.46×10^7	6.99×10^7	1.24×10^8	1.99×10^8	2.96×10^8	4.16×10^8	5.60×10^8
k_{RP}	3.88×10^{-14}	2.98×10^{-14}	2.44×10^{-14}	2.10×10^{-14}	1.88×10^{-14}	1.73×10^{-14}	1.63×10^{-14}
			Triplet Reaction Pathways				
K_{eq}	7.90×10^{-22}	3.20×10^{-22}	1.56×10^{-22}	8.73×10^{-23}	5.44×10^{-23}	3.67×10^{-23}	2.65×10^{-23}
TS1-T							
Γ	6.78	5.24	4.26	3.59	3.12	2.77	2.51
k_2	9.32×10^{10}	9.25×10^{10}	9.24×10^{10}	9.24×10^{10}	9.27×10^{10}	9.32×10^{10}	9.40×10^{10}
k_{RP}	7.36×10^{-11}	2.96×10^{-11}	1.44×10^{-11}	8.06×10^{-12}	5.04×10^{-12}	3.42×10^{-12}	2.49×10^{-12}
TS1′-T							
Γ	2.77x 10^2	1.35×10^2	7.56×10^1	4.69×10^1	3.16×10^1	2.26×10^1	1.70×10^1
k_2	6.86×10^{10}	7.24×10^{10}	7.62×10^{10}	8.01×10^{10}	8.42×10^{10}	8.82×10^{10}	9.26×10^{10}
k_{RP}	5.42×10^{-11}	2.32×10^{-11}	1.19×10^{-11}	6.99×10^{-12}	4.57×10^{-12}	3.24×10^{-12}	2.45×10^{-12}
			All Reaction Pathways[a]				
k_{TOTAL}[b]	1.11×10^{-11}	5.85×10^{-12}	3.57×10^{-12}	2.41×10^{-12}	1.78×10^{-12}	1.40×10^{-12}	1.15×10^{-12}
k_{TOTAL}[c]	1.28×10^{-10}	5.29×10^{-11}	2.63×10^{-11}	1.51×10^{-11}	9.64×10^{-12}	6.68×10^{-12}	4.96×10^{-12}
exp[d]	1.22×10^{-11}	8.61×10^{-12}	6.48×10^{-12}	5.12×10^{-12}	4.19×10^{-12}	3.53×10^{-12}	3.04×10^{-12}

[a] Sum of the k_{RP} calculated for the five reaction pathways. [b] Without tunneling correction. [c] With tunneling correction. [d] Reference 56.

At the CASPT2 level of theory **TS1-T** is calculated to be 2.5 kcal/mol less energetic than **TS1′-T** (see ΔU values in Table 1), whereas at the CASSCF(12,10) level this energy difference is calculated to be only 1.1 kcal/mol (see Table S1, Supporting Information). As mentioned earlier for the direct H-atom transfer on the singlet PES, the lower energy of **TS1-T** with respect to **TS1′-T** is attributed to an intermolecular noncovalent O···O bonding interaction between this pair of atoms, which is lacking in **TS1′-T**. However in the case of **TS1-T** such interaction is weaker than that found for **TS1-S** because the O1−O3 distance in **TS1-T** (3.026 Å) is significantly longer than in **TS1-S** (2.271 Å). The long O1−O3 distance in **TS1-T** is related to the wider O2−H1−O4 angle in **TS1-T** (176.0°) as compared with **TS1-S** (145.8°).

The direct H-atom transfer from **2** to **1** on the triplet PES through the lowest energy transition structure **TS1-T** involves a $\Delta E^{\ddagger}$(0 K) of −3.8 kcal/mol (see Table 1). We note that this activation energy is close to that (−3.43 kcal/mol) obtained from the ZPVE-corrected CCSD(T)/cc-pVDZ//B3LYP/6-311G(d,p) energies reported by Hou and Wang.[8]

The IRC calculations showed that both **TS1-T** and **TS1′-T** go backward to the hydrogen-bonded complex **CX-T** and go forward to give the products **3** plus $^3\mathbf{O_2}$. According to Table 1, the H-atom transfer from **2** to **1** leading to the formation of the latter products is predicted to involve an energy of reaction of −36.9 kcal/mol at 0 K. Inclusion of the thermal correction to enthalpy leads to the same value for the ΔH_r(298 K), which is in reasonable agreement with the ΔH_f(298 K) of −38.0 kcal/mol derived from experimental enthalpies of formation.[6]

3.3.3. Stepwise Mechanism. The geometry optimization of the lowest energy triplet state of the CH_3OOOOH adduct was found to lead to the hydrogen-bonded complex **CX-T** without surmounting an energy barrier. Therefore, it turns out that the CH_3OOOOH tetraoxide is not an energy minimum on the triplet PES. As a result, the hypothetical stepwise mechanism "A" (Scheme 1) can be discarded on the triplet PES.

In summary, the direct H-atom transfer from $HO_2^\bullet$ to $CH_3O_2^\bullet$ appears to be the most viable pathway for reaction eq 4 on the triplet PES. If one assumes that such H-atom transfer takes place through the lowest energy transition structure **TS1-T**, then a $\Delta E^{\ddagger}$(0 K) of −3.8 kcal/mol is predicted for this reaction. This activation energy is 9.3 kcal/mol lower than that calculated for the direct H-atom transfer on the singlet PES via the **TS1-S** transition structure. Consequently, it can be concluded that the direct H-atom transfer on the triplet PES is the dominant pathway for reaction eq 4.

At this point it is worth mentioning that the mechanism predicted for reaction eq 4 is analogous to that predicted by Zhu and Lin[37] for the self-reaction of $HO_2^\bullet$. These authors explored the singlet and triplet PESs of the H_2O_4 reaction system at the B3LYP/6-311G(d,p) level of theory and calculated the relative energies of the stationary points with the G2M method to approximate the CCSD(T)/6-311+G(3df,2p) level of theory. The results of the calculations showed that the most favored product reaction pathway, producing hydrogen peroxide (HOOH) and O_2, occurs by the formation of a triplet hydrogen-bonded six-membered-ring complex through head-to-tail association, lying 9.5 kcal/mol below the reactants. This complex fragments to give HOOH and $^3O_2$ via a transition structure showing a geometry similar to that of **TS1-T**, which lies below the reactants by about 0.5 kcal/mol. More recently, Donaldson and Francisco[38] have found the same six-membered-ring complex and transition structure on the triplet PES calculated at the QCISD/6-311G(2df,2p) level of theory for the reaction of $^3O_2$ with HOOH leading to the formation of two molecules of $HO_2^\bullet$.

3.4. Kinetics. With the main purpose of showing a qualitative description of the experimental trend concerning the strong negative temperature dependence for reaction eq 4, we carried

out standard transition state theory calculations for the reaction pathways that may contribute to the overall rate constant measuring the rate of $CH_3O_2^{\bullet}$ disappearance. In the previous sections it has been shown that all these reaction pathways on both the singlet and triplet PESs consist of a reversible first step involving the barrierless formation of a prereactive complex (**CX-S** or **CX-T**), followed by the irreversible formation of products (i.e., $CH_3OOH + {}^1O_2$, or CH_3OOOOH, or $CH_3OOH + {}^3O_2$). Therefore, each reaction pathway is a two-step process as described by eq 5, where the corresponding complex is in equilibrium with the reactants

$$CH_3O_2^{\bullet} + HO_2^{\bullet} \underset{k_{-1}}{\overset{k_1}{\rightleftharpoons}} \text{complex} \xrightarrow{k_2} \text{products} \qquad (5)$$

If k_1 and k_{-1} are the rate constants for the first step and k_2 is the rate constant for the second, a steady-state analysis leads[52] to a rate constant for the reaction pathway under consideration, denoted as k_{RP}, which can be approximated as

$$k_{RP} = \frac{k_1}{k_{-1}} k_2 = K_{eq} k_2 \qquad (6)$$

where K_{eq} stands for the equilibrium constant in the first step, which can be written as

$$K_{eq} = \frac{Q_{CX}}{Q_{CH_3O_2} Q_{HO_2}} e^{-(E_{CX} - E_R)/(RT)} \qquad (7)$$

where the various Qs are the partition functions of the reactants ($Q_{CH_3O_2^{\bullet}}$ and $Q_{HO_2^{\bullet}}$) and prereactive complex (Q_{CX}); E_R and E_{CX} are the total electronic energy plus the ZPVE of the reactants and prereactive complex, respectively; R is the ideal gas constant; and T is the absolute temperature. The rate constant k_2 can be evaluated using the standard transition state theory equation:[53]

$$k_2 = \Gamma \frac{k_b T}{h} \frac{Q_{TS}}{Q_{CX}} e^{-(E_{TS} - E_{CX})/(RT)} \qquad (8)$$

where Q_{TS} and E_{TS} are the partition function and the total electronic energy plus ZPVE, respectively, of the transition state and Γ is the tunneling factor.

According to the standard formulas,[22] the Qs were evaluated using the CASSCF/6-31+G(3df,2p)-optimized geometries and harmonic vibrational frequencies, while the Es were taken as the ZPVE-corrected CASPT2/6-311+G(3df,2p) total energies. The Γs were evaluated by zero-order approximation to the vibrationally adiabatic PES model with zero curvature.[54] In this approximation the tunneling is assumed to occur along a unidimensional minimum energy path. The potential energy curve is approximated by an unsymmetrical Eckart potential energy barrier[55] that is required to go through the ZPVE corrected energy (denoted as E) of the reactants, transition state, and products. The equations that describe the Eckart potential energy function were adapted from Truong and Truhlar.[54] Solving the Schroedinger equation for the Eckart function yields the transmission probability, $\kappa(E)$. Then Γ is obtained by integrating the respective $\kappa(E)$ over all possible energies:

$$\Gamma(T) = \frac{1}{k_b T} e^{(E_{TS} - E_{CX})/(RT)} \int_0^{\infty} e^{-E_{TS}/(RT)} \kappa(E)\, dE \qquad (9)$$

Table 2 lists the values of K_{eq}, Γ, k_2, and k_{RP} for the five reaction pathways considered in this study, along with the overall rate constant, denoted as k_{TOTAL}, calculated in the range of temperatures between 225 and 375 K. This range of temperatures was chosen thinking on the interest of reaction eq 4 in environmental science. The most recent experimental values[56] of the rate constant for this reaction are also included in Table 2.

First we note that the contribution to k_{TOTAL} of the three reaction pathways considered on the singlet PES is negligible. In the case of the two direct H-atom-transfer pathways, this result is a consequence of the large energy barrier predicted for these pathways, as compared with those calculated for the two direct H-atom-transfer pathways on the triplet PES. As regards the third pathway on the singlet PES, its contribution to k_{TOTAL} is negligible because the values of Γ are calculated to be very close to 1. Second we note that the value of 15.1×10^{-12} cm^3 molecule^{-1} s^{-1} calculated for k_{TOTAL} at 300 K is roughly in reasonable agreement with the experimental value of 5.12×10^{-12} cm^3 molecule^{-1} s^{-1}, differing by a factor of 2.9. Interestingly enough, the k_{TOTAL} values calculated without tunneling correction are underestimated as compared to the experimental values by a factor ranging from 1.1 to 2.6 when going from 225 to 375 K. On the other hand, the k_{TOTAL} values calculated with tunneling correction are overestimated with respect to the experimental values by a factor ranging from 10.5 to 1.6 when passing from 225 to 375 K. Therefore, it is likely that the tunneling corrections employed here are overestimated. This feature is more pronounced at low temperatures.

In good agreement with experimental findings, the results listed in Table 2 predict significant negative temperature dependence for the overall rate constant in the range of temperatures considered. This trend is observed for the k_{TOTAL} values calculated either with or without tunneling correction. Since the values of k_2 increase with the temperature while the values of K_{eq} decrease, it can be concluded that the negative temperature dependence predicted for the overall rate constant is related to the formation of the prereactive diradical complex along all the reaction pathways considered in this study.

4. Summary and Conclusions

In an attempt to understand the mechanism of the reaction of alkylperoxy radicals with $HO_2^{\bullet}$, a key reaction in both atmospheric and combustion environments, the singlet and triplet potential energy surfaces for the gas-phase reaction between $CH_3O_2^{\bullet}$ and $HO_2^{\bullet}$ leading to the formation of CH_3OOH and O_2 have been investigated from the theoretical point of view by means of quantum-mechanical electronic structure methods (CASSCF and CASPT2). In addition, standard transition state theory calculations have been carried out with the main purpose of a qualitative description of the strong negative temperature dependence observed for this reaction. From the analysis of the results, the following main points emerge.

(1) All the reaction pathways on both the singlet and triplet potential energy surfaces consist of a reversible first step involving the barrierless formation of a hydrogen-bonded prereactive complex in the entrance channel, followed by the irreversible formation of products. This complex is a diradical species where the two unpaired electrons are not used for bonding and lies about 5 kcal/mol below the energy of the reactants at 0 K.

(2) The lowest energy reaction pathway occurs on the triplet PES and leads to the formation of CH_3OOH and O_2 ($^3\Sigma_g^-$). It involves the direct H-atom transfer from HO_2 to CH_3O_2 in the diradical complex through a transition structure lying 3.8 kcal/mol below the energy of the reactants at 0 K.

(3) Contradicting the currently accepted interpretation of the reaction mechanism, the observed strong negative temperature dependence of the rate constant is due to the formation of the hydrogen-bonded diradical complex rather than a short-lived tetraoxide intermediate CH_3OOOOH.

Acknowledgment. This research was supported by the Spanish DGI (Grant CTQ2005-07790). Additional support came from Catalonian CIRIT (Grant 2005SGR00111). The larger calculations described in this work were performed at the Centre de Supercomputació de Catalunya (CESCA).

Supporting Information Available: The Cartesian coordinates of all structures reported in this paper and a table summarizing total energies, zero-point vibrational energies, absolute entropies, and thermal corrections to enthalpy and Gibbs free energy. This material is available free of charge via the Internet at http://pubs.acs.org.

References and Notes

(1) Lightfoot, P. D.; Cox, R. A.; Crowley, J. N.; Destriau, M.; Hayman, G. D.; Jenkin, M. E.; Moortgat, G. K.; Zabel, F. *Atmos. Environ. Part A* **1992**, *26A*, 1805−1961.

(2) Wallington, T. J. Dagaut, P.; Kurrylo, M. J. *Chem. Rev.* **1992**, *92*, 667−710.

(3) Lesclaux, R. Combination of peroxyl radicals in the gas phase. In *Peroxyl Radicals*; Alfassi, Z. B., Ed.; John Wiley & Sons: New York, 1997; pp 81−112.

(4) Wallington, T. J.; Nielsen. O. J.; Sehested, J. Reactions of organic peroxy radicals in the gas phase. In *Peroxyl Radicals*; Alfassi, Z. B., Ed.; John Wiley: New York, 1997; pp 113−172.

(5) Finlayson-Pitts, B. J.; Pitts, J. N., Jr. *Chemistry of the Upper and Lower Atmosphere*; Academic: New York, 2000; Chapter 6.

(6) Tyndall, G. S.; Cox, R. A.; Granier, C.; Lesclaux, R.; Moortgat, G. K.; Pilling, M. J.; Ravishankara, A. R.; Wallington, T. J. *J. Geophys. Res.* **2001**, *106*, 12157−12182.

(7) Boyd, A. A.; Flaud, P. M.; Daugey, N.; Lesclaux, R. *J. Phys. Chem. A* **2003**, *107*, 818−821.

(8) Hou, H.; Wang, B. *J. Phys. Chem. A* **2005**, *109*, 451−460.

(9) For a review, see: Roos, B. O. *Adv. Chem. Phys*. **1987**, *69*, 399.

(10) Frisch, M. J.; Pople, J. A.; Binkley, J. S. *J. Chem. Phys.* **1984**, *80*, 3265.

(11) Hehre, W. J.; Radom, L.; Schleyer, P, v. R.; Pople, J. A. *Ab Initio Molecular Orbital Theory;* John Wiley: New York, 1986; pp 86−87.

(12) Schlegel, H. B. *J. Comput. Chem*. **1982**, *3*, 214.

(13) Bofill, J. M. *J. Comput. Chem.* **1994**, *15*, 1.

(14) Anglada, J. M.; Bofill, J. M. *Theor. Chim. Acta* **1995**, *92*, 369.

(15) (a) Fukui, K. *Acc. Chem. Res.* **1981**, *14*, 363. (b) Ishida, K.; Morokuma, K.; Kormornicki, A. *J. Chem. Phys.* **1977**, *66*, 2153.

(16) (a) Gonzalez, C.; Schlegel, H. B. *J. Chem. Phys.* **1989**, *90*, 2154. (b) Gonzalez, C.; Schlegel, H. B. *J. Phys. Chem.* **1990**, *94*, 5523.

(17) Schmidt, M. W.; Baldrige, K. K.; Boatz, J. A.; Elbert, S. T.; Gordon, M. S.; Jensen; J.; Koseki, S.; Matsunaga, N.; Nguyen, K. A.; Su, S.; Windus, T. L.; Dupuis, M.; Montgomery, J. A. *J. Comput. Chem.* **1993**, *14*, 1347.

(18) (a) Anderson, K.; Malmqvist, P.-A.; Roos, B. O.; Sadlej, A. J.; Wolinski, K. *J. Phys. Chem.* **1990**, *94*, 5483. (b) Anderson, K.; Malmqvist, P.-A.; Roos, B. O. *J. Chem. Phys.* **1992**, *96*, 1218.

(19) Anderson, K. *Theor. Chim. Acta* **1995**, *91*, 31.

(20) Boys, S. F.; Bernardi, F. *Mol. Phys.* **1970**, *19*, 553.

(21) Andersson, K., Barysz, M.; Bernhardsson, A.; Blomberg, M. R. A.; Cooper, D. L.; Fleig, T.; Fülscher, M. P.; DeGraaf, C.; Hess, B. A.; Karlström, G.; Lindh, R.; Malmqvist, P.-Å.; Neogrády, P.; Olsen, J.; Roos, B. O.; Sadlej, A. J.; Schütz, M.; Schimmelpfennig, B.; Seijo, L.; Serrano-Andrés, L.; Siegbahn, P. E. M.; Stålring, J.; Thorsteinsson, T.; Veryazov, V.; Widmark, P.-O. *MOLCAS*, version 5; Lund University: Lund, Sweden, 2000.

(22) See, e.g.: McQuarrie, D. *Statistical Mechanics;* Harper and Row: New York, 1986.

(23) (a) Biegler-König, F. W.; Bader, R. F. W.; Tang, T.-H. *J. Comput. Chem.* **1982**, *3*, 317. (b) Bader, R. F. W.; Tang, T.-H.; Tal, Y.; Biegler-König, F. W. *J. Am. Chem. Soc.* **1982**, *104*, 946.

(24) Bader, R. F. W. *Atoms in Molecules: A Quantum Theory*; Clarendon: Oxford, UK, 1990.

(25) Bair, R. A.; Goddard, W. A., III. *J. Am. Chem. Soc.* **1982**, *104*, 2719.

(26) Cohen, D.; Basch, H.; Osman, R. *J. Chem. Phys.* **1984**, *80*, 5684.

(27) Jackels, C. F.; Philips, D. H. *J. Chem. Phys.* **1986**, *84*, 5013.

(28) Besler, B. H.; Sevilla, M. D.; MacNeille, P. *J. Phys. Chem.* **1986**, *90*, 6446.

(29) Boyd, S. L.; Boyd, R. J.; Barclay, L. R. C. *J. Am. Chem. Soc.* **1990**, *112*, 5724.

(30) Francisco, J. S.; Zhao, *Mol. Phys.* **1991**, *72*, 1207.

(31) Green, W. H. *Int. J. Quantum Chem.* **1994**, *52*, 8327.

(32) Shen, D.; Moise. A.; Pritchard, H. O. *J. Chem. Soc., Faraday Trans.* **1995**, *91*, 1425.

(33) Henon, E.; Bohr, F.; Chakir, A. Brion, J. *Chem. Phys. Lett.* **1997**, 557.

(34) Jursic, B. S. *J. Phys. Chem. A* **1997**, *101*, 2345.

(35) Aplincourt, P.; Ruiz-López, M. F.; Assfeld, X.; Bohr, F. *J. Comput. Chem.* **1999**, *20*, 1039.

(36) Bohr, F.; Henon, E.; García, I.; Castro, M. *Int. J. Quantum Chem.* **1994**, *75*, 671.

(37) Zhu, R.; Lin, M. C. *PhysChemComm.* **2001**, *23*, 1.

(38) Donaldson, D. J.; Francico, J. S. *Phys. Chem. Chem. Phys.* **2003**, *5*, 3183.

(39) Feria, L.; Gonzalez, C.; Castro, M. *Int. J. Quantum Chem.* **2004**, *96*, 380.

(40) Lubic, K. G.; Amano, T. *J. Chem. Phys.* **1984**, *81*, 4826.

(41) Wallington, T. J.; Hurley, M. D.; Schneider, W. F.; Sehested, J.; Nielsen, O. J. *Chem. Phys. Lett.* **1994**, *218*, 34.

(42) Hezberg, G. *Spectra of Diatomic Molecules*, 2nd ed.; McGraw-Hill: New York, 1950.

(43) Beckwith, A. L. J.; Ingold, K. U. In *Rearrangements in Ground and Excited States*; de Mayo, P., Ed.; Academic Press: New York; Vol. 1.

(44) Pauling, L. C. *The Nature of the Chemical Bond*; Cornell University Press: Ithaca, NY, 1960.

(45) Cioslowski, J.; Mixon, S. T.; Fleischmann, E. D. *J. Am. Chem. Soc.* **1991**, *113*, 4751.

(46) Bofill, J. M.; Olivella, S.; Sole, A.; Anglada, J. M. *J. Am. Chem. Soc.* **1999**, *121*, 1337.

(47) Gibbs, G. V.; Boisen. M. B.; Rosso, K. M.; Teter, D. M.; Bukowinsky, M. S. T. *J. Phys. Chem. B* **2000**, *104*, 10534.

(48) Zhurova, E. A.; Tsirelson, V. G.; Stash, A. I.; Pinkerton, A. A. *J. Am. Chem. Soc.* **2002**, *124*, 4574.

(49) Alkorta, I.; Elguero, J. *J. Chem. Phys.* **2002**, *117*, 6463.

(50) Wallington, T. J.; Hurley, M. D.; Schneider, W. F. *Chem. Phys. Lett.* **1996**, *251*, 164.

(51) Catoire, V.; Lesclaux, R.; Schneider, W. F.; Wallington, T. J. *J. Phys. Chem.* **1996**, *100*, 14356.

(52) Singleton, D. L.; Cvetanovic, R. J. *J. Am. Chem. Soc.* **1976**, *98*, 6812.

(53) Eyring, H. *J. Chem. Phys.* **1935**, *107*, 107.

(54) Truong, T. N.; Truhlar, D. G. *J. Chem. Phys.* **1990**, *93*,1761.

(55) Eckart, C. *Phys. Rev.* **1930**, *35*, 1303.

(56) Atkinson, R.; Baulch, D. L.; Cox, R. A.; Hampson, R. F.; Kerr, J. A.; Rossi, M. J.; Troe, J. *J. Phys. Chem. Ref. Data* **1997**, *26*, 521.